

# Chemical evolution during gas-rich galaxy interactions

Josefa Perez,<sup>1,2,3★</sup> Leo Michel-Dansac<sup>4</sup> and Patricia B. Tissera<sup>1,3</sup>

<sup>1</sup>*Instituto de Astronomía y Física del Espacio, Conicet-UBA, CC67, Suc.28, Ciudad de Buenos Aires, Argentina*

<sup>2</sup>*Cátedra de Astronomía General, Facultad de Ciencias Astronomía y Geofísica, Universidad Nacional de La Plata, Argentina*

<sup>3</sup>*Consejo Nacional de Investigaciones Científicas y Técnicas, CONICET, Argentina*

<sup>4</sup>*Centre de Recherche Astrophysique de Lyon, Université de Lyon, Université Lyon 1, Observatoire de Lyon, Ecole Normale Supérieure de Lyon, CNRS, UMR 5574, 9 avenue Charles André, Saint-Genis Laval, 69230, France*

Accepted 2011 June 1. Received 2011 May 9; in original form 2011 February 23

## ABSTRACT

We perform and analyse a set of galaxy interactions performed by using a self-consistent chemo-hydrodynamical model which includes star formation, supernova (SN) feedback and chemical evolution. In agreement with previous works, we find that tidally induced low-metallicity gas inflows dilute the central oxygen abundance and contribute to the flattening of the metallicity gradients. The tidally induced inflows trigger starbursts which increase the impact of Type II supernova (SN II) feedback injecting new chemical elements and driving galactic winds which modulate the metallicity distribution. Although  $\alpha$ -enhancement in the central regions is detected as a result of the induced starbursts in agreement with previous works, our simulations suggest that this parameter can only provide a timing of the first pericentre mainly for non-retrograde encounters. In order to reproduce wet major mergers at low and high redshifts, we have run simulations with respectively 20 and 50 per cent of the disc in the form of gas. We find that the more gas-rich encounters behave similarly to the less rich ones, between the first and second pericentre, where low-metallicity gas inflows are triggered. However, the higher strength of the inflows triggered in the more gas-rich interactions produces larger metal dilution factors, which are modulated afterwards by the new chemical production by SN. We find that the more gas-rich interaction develops violent and clumpy star formation triggered by local instabilities all over the disc before the first pericentre, so that if these galaxies were observed at these early stages where no important tidally induced inflows have been able to be developed yet, they would tend to show an excess of oxygen. We find a global mean correlation of both the central abundances and the gradients with the strength of the star formation activity. However, the correlations are affected by orbital parameters, gas inflows and outflows, suggesting that it might be difficult to determine it from observations. Overall, our findings show that a consistent description of the gas dynamics and stellar evolution along the interactions is necessary to assess their effects on the chemical properties of the interstellar medium.

**Key words:** galaxies: abundances – galaxies: evolution – galaxies: formation – galaxies: interactions.

## 1 INTRODUCTION

Galaxy interactions are considered a key process in galaxy formation since these violent events could be able to redistribute mass and angular momentum very efficiently (e.g. Barnes & Hernquist 1996; Tissera 2000; Di Matteo et al. 2008). As a consequence, chemical elements can be stirred up affecting their distribution and metallicity patterns such as gradients. There are numerous observational works

dedicated to the study of galaxy pairs (e.g. Sérsic & Pastoriza 1967; Tinsley & Larson 1978; Barton, Geller & Kenyon 2000; Lambas et al. 2003; Nikolic, Cullen & Alexander 2004; Alonso et al. 2006; Woods, Geller & Barton 2006; Ellison et al. 2008, 2010; Patton et al. 2011). But only in the last few years, it has been possible to focus on the effects of galaxy interactions on chemical abundances. Interacting galaxies, galaxy pairs, ultra-luminous infrared galaxies, and merger remnants have been found to exhibit low gas-phase metallicity at a given stellar mass compared with the mean mass–metallicity relation (e.g. Kewley, Geller & Barton 2006; Ellison et al. 2008; Michel-Dansac et al. 2008; Rupke, Veilleux & Baker

★E-mail: jperez@fcaglp.unlp.edu.ar

2008; Peebles, Pogge & Stanek 2009; Sol Alonso, Michel-Dansac & Lambas 2010). Recently, Kewley et al. (2010) analysed the metallicity gradients of galaxy pairs in detail confirming the central dilution and gradient flattening previously reported by several authors. These trends have been interpreted as a consequence of low-metallicity inflows triggered by galaxy interactions. Indeed, these interacting galaxies are in majority spirals which, in the nearby Universe, hold a gas-phase metallicity gradient (e.g. Zaritsky, Kennicutt & Huchra 1994; Dutil & Roy 1999; Moustakas et al. 2010). The presence of metallicity gradients could explain the decrease of the central abundances when low-metallicity inflows are triggered during interactions. There are also some galaxies in pairs with abundances departing significantly from the mass–metallicity relation such as those reported by Michel-Dansac et al. (2008), Peebles et al. (2009) and Sol Alonso et al. (2010). Hence, there are still effects of galaxy interactions which demand further understanding.

By using cosmological chemo-hydrodynamical simulations, Perez et al. (2006) showed for the first time that the interacting galaxies tend to have lower central metallicity when compared to isolated galaxies of similar stellar mass. These authors showed that the decrease of central abundances could be explained in terms of gas inflows triggered during the interactions. More recently, other numerical works have confirmed these findings by using different simulations and hypothesis (Montuori et al. 2010; Rupke, Kewley & Barnes 2010a). Particularly, Rupke et al. (2010a) studied the evolution of metallicity profiles by using hydrodynamical simulations to recreate the major interaction of galaxies with a gas mass fraction similar to that used in our less gas-rich simulations. However, these authors did not consider new star formation (SF) activity and the subsequent chemical enrichment of the interstellar medium (ISM) as we do in our work.

In this paper, we use a chemical model grafted on to GADGET-2, which allows the description of the chemical enrichment of baryons as the merger evolves. Our code also includes a self-consistent model of supernova (SN) feedback (Scannapieco et al. 2006), so mass-loaded galactic outflows can be triggered without including mass-dependent parameters. This code includes the chemical model of Mosconi et al. (2001), which describes the enrichment of baryons by supernovae Types Ia and II (SNe Ia/II). Hence, the simulations analysed in this work follow the dynamical evolution together with the chemical evolution of baryons as the interaction takes place.

This paper is organized as follows. In Section 2, we describe the code and the initial conditions designed for this work. In Section 3, we explore wet interactions at low redshift, while Section 4 analyses a more gas-rich encounter in order to reproduce typical wet interactions at high redshift. Finally, we summarize our findings in Section 5.

## 2 NUMERICAL SIMULATIONS

We performed a set of hydrodynamical simulations of interacting pre-prepared disc galaxies of comparable masses. The simulations were run by using a version of GADGET-2 (Springel 2005) modified by Scannapieco et al. (2005, 2006) to include the chemical model of Mosconi et al. (2001) and a new SN feedback model developed to provide an improved description of the ISM and the injection of energy and metals generated by SNe. The multiphase and SN feedback model developed by Scannapieco et al. (2005, 2006) allows the coexistence of gas clouds with different thermodynamical properties and is able to describe the injection of energy from young stars into the ISM producing the self-regulation of the SF activity as well as triggering galactic outflows without the need

**Table 1.** Characteristics of the numerical experiments.  $i$ : angle between the two total angular momenta of the galaxies.  $E_{\text{SN}}$ : amount of SN energy released by each event.  $f_{\text{gas}}$ : gas fraction of the discs.

Simulation	$i$ ( $^\circ$ )	$E_{\text{SN}}$ ( $10^{51}$ erg s $^{-1}$ )	$f_{\text{gas}}$
SimI	45	0.5	0.20
SimII	0	0.5	0.20
SimIII (no SF)	0	0	0.20
SimIV	0	0.04	0.20
SimV	180	0.5	0.20
SimVI	0	0.5	0.50

to introduce mass-dependent parameters or to change discontinuous particle momentum to start a wind or temporary suppression of radiative cooling. This scheme has been successful at reproducing the SF activity during quiescent and starburst phases and is able to trigger mass-loaded winds with strength dependent on the potential well of the systems (e.g. Scannapieco et al. 2006; De Rossi, Tissera & Pedrosa 2010; Sawala et al. 2011; Scannapieco et al. 2011).

Chemical elements are synthesized in the stellar interiors and ejected into the ISM by SNe. The chemical model describes the enrichment by SN II and SN Ia, providing information on certain individual chemical elements. We also assume that each SN injects an amount of energy into the ISM,  $E_{\text{SN}}$  (cf. Table 1). SN II and SN Ia are originated from different progenitors with different rates, yields and time-scales. We assume that SNe II are generated by stars more massive than  $8 M_{\odot}$  after  $\approx 10^6$  yr. We adopt the yields given by Woosley & Weaver (1995). For SN Ia, the chemical model assumes lifetimes randomly distributed in the range ( $10^8$  and  $10^9$ ) yr and yields from W7 model of Thielemann, Nomoto & Hashimoto (1993). The SN feedback model is able to generate galactic outflows powerful enough to transport enriched material outside the galaxies (Scannapieco et al. 2008). Thus, these simulations provide us with the evolution of the dynamical and the chemical properties of the baryons as galaxy interactions proceed.

We run three major merger simulations (1:1) varying the orbital parameters (SimI, SimII and SimV) with the same SF and SN feedback model. We also performed a run (SimIV) with the same initial conditions as SimII, but decreasing the energy release by each SN event ( $E_{\text{SN}}$ ), and a run (SimIII) with the same orbital parameters, but without SF and feedback activity. This last experiment is comparable to those analysed by Rupke et al. (2010a). In order to represent wet mergers at low redshift, these experiments (from SimI to SimV) were run with a 20 per cent of the disc in form of gas. Finally, SimVI has the same orbital, SF and feedback parameters as SimII, but the gas fraction in the disc has been increased up to 50 per cent in order to simulate a wet encounter at high redshift. The parameters of the simulations are summarized in Table 1.

Initial conditions correspond to disc galaxies composed of a dark matter (DM) halo, a bulge component (modelled by an NFW profile and a Hernquist profile, respectively) and an exponential disc, with a total baryonic mass of  $M_b \sim 5 \times 10^{10} M_{\odot}$ . For the less gas-rich simulations, we use 200 000 DM particles, 100 000 stars distributed in the stellar disc and the bulge, and 100 000 particles to represent the disc gas component with an initial gas resolution of  $\approx 3 \times 10^5 M_{\odot}$ . For the more gas-rich experiment, we re-calculate the number of particles so as to keep similar mass resolution. Total stellar masses change according to the gas content in the galaxy discs, being  $M_{\star} \sim 4.4 \times 10^{10} M_{\odot}$  for the less gas-rich experiment and  $M_{\star} \sim 3.2 \times 10^{10} M_{\odot}$  for the more gas-rich simulation. A gravitational

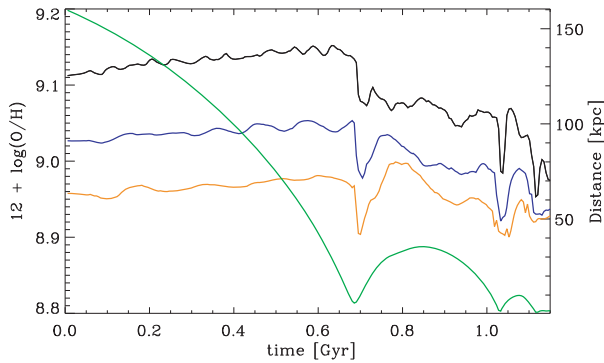


**Figure 1.** Evolution of the gas-phase oxygen abundance measured inside a sphere of 2 kpc (black line), 4 kpc (blue line) and 6 kpc (orange line) radius for one of the interacting galaxies of SimI. The relative distance between the centre of mass of the simulated galaxies is also plotted (green line).

softening of  $\epsilon_G = 0.16$  kpc was adopted for the gas particles,  $\epsilon_S = 0.2$  kpc for the stars and  $\epsilon_{DM} = 0.32$  kpc for the DM. Galaxies live in DM haloes with circular velocities of  $160 \text{ km s}^{-1}$ . All these experiments are set to have the same elliptical orbits, according to Toomre & Toomre (1972), with the pericentre distance of  $\approx 20$  kpc and the circularity parameter  $\epsilon \sim 0.20$ . These orbital values are consistent with those obtained from the analysis of cosmological simulations (e.g. Khochfar & Burkert 2006). We have kept them fixed so that changes in the chemical and dynamical properties can only be ascribed to the different angular momentum orientation. A larger orbital distribution might be of interest to analyse possible dependences in the future.

The gas component is initially assumed to have been pre-enriched by the existing stars, following a metallicity gradient statistically consistent with observations. We assigned an initial amount of chemical elements to the gas particles in order to reproduce the mean observational gradient reported by Dutil & Roy (1999), which for the less gas-rich simulations is  $-0.08 \text{ dex kpc}^{-1}$  with a central oxygen abundance of 9.2. Thus, the initially simulated galaxies are located on to the observed mass–metallicity relation (Tremonti et al. 2004). For the more gas-rich simulation (SimVI), the initial metallicity gradient is somewhat steeper ( $-0.1 \text{ dex kpc}^{-1}$ ) and the central metallicity is lower (by 0.7 dex) than the less gas-rich galaxies. By doing that, these more gas-rich simulated galaxies are then initially on to the mass–metallicity relation observed at high redshift by Maiolino et al. (2008). Note that the exact adopted values are not critical since we are interested in the relative evolution of the metallicity.

### 3 METALLICITY EVOLUTION OF WET MERGERS IN THE LOCAL UNIVERSE

In this section, we analyse the effects of galaxy interactions on the central metallicity in wet local encounters. Taking SimI as an example, we show in Fig. 1 the evolution of the gas-phase O/H abundance of one member of the galaxy pair<sup>1</sup> as the interaction proceeds. The evolution of the interaction can be followed by the relative distances between the centre of masses of the interacting systems, plotted in the same figure. As can be seen, there is a clear evidence of a decrease in the central gas-phase metallicity which can be correlated with the first and the second pericentres.

<sup>1</sup> The other member of the pair has a similar behaviour.

Several previous works have shown that during a close encounter, strong tidal torques can develop, re-distributing angular momentum and producing gas infall (e.g. Barnes & Hernquist 1996; Mihos & Hernquist 1996; Tissera 2000; Di Matteo et al. 2008). In the case that a metallicity gradient exists, the infalling gas will tend to have lower metallicity than that of baryons in the central region producing a dilution as is clearly shown by our simulation (see also Montuori et al. 2010; Rupke et al. 2010a).

In order to quantify the chemical changes as a function of time, we compute the central abundances inside concentric spheres of different radius in the range from 1 to 10 kpc. As an example, Fig. 1 shows the gas-phase oxygen abundance measured inside a sphere of 2, 4 and 6 kpc of radius. As can be appreciated, as one moves inwards, the signals get noisier since the number of particle decreases. If one moves to a larger radius, the signal decreases as chemical abundances start to be dominated by the external regions. As a compromise between these two effects, we select  $R_{\text{cen}} = 4$  kpc (blue line) to define the central region, where we will perform the analysis of central metallicities.

In order to understand the decrease in the central abundances shown by Fig. 1, we analyse the evolution of the central gas inflows and their abundances. At any given time, we compute the central gas inflow as the mass ratio of the new accreted gas within  $R_{\text{cen}}$  to the total gas content within the same radius. Fig. 2(a) shows the evolution of this central gas inflow as the interacting galaxies approach each other. We find that the gas inflow remains constant in around 2 per cent until the first close passage when it rises up to  $\sim 8$  per cent. From the second pericentre, the gas inflow steadily increases up to around 30 per cent. This gas inflow is dominated by low-metallicity material as can be appreciated from Fig. 2(b) (solid line), where we plot its O/H abundance. The accretion of this low-metallicity gas dilutes the central oxygen abundance as shown by the continuous decrease detected after the first pericentre (Fig. 2b, dotted line). The main drops in central abundances correlate with the occurrence of the pericentres driven by important gas inflows

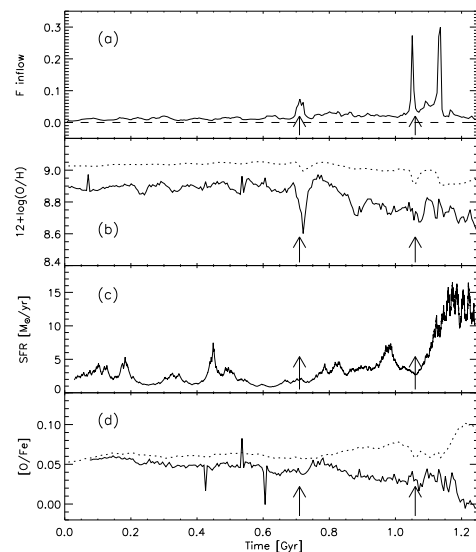


**Figure 2.** Evolution of gas inflow and of chemical abundances in the central region  $R < R_{\text{cen}}$  of one galaxy in SimI. (a) Fraction of the gas falling within  $R_{\text{cen}}$  as a function of time. The dashed horizontal line represents the initial fraction. (b) Oxygen abundance of the infalling gas (solid) and the mean central abundance within  $R_{\text{cen}}$  (dotted line). (c) Evolution of the SFR. (d)  $\alpha$ -enhancement of the infalling gas (solid) and its mean central value (dotted line). Arrows indicate the first and second pericentres.

(Fig. 2a). Additionally, the gas inflow is also responsible for triggering new SF activity (Fig. 2c). In SimI, the star formation rate (SFR) increases by a factor of 3 from the first pericentre as the interaction continues fuelling the gas inflow (Figs 2a and c). As a consequence of this increase in the SFR, the enrichment by SN II also increases, diminishing the effects of chemical dilution previously imprinted by the low-metallicity gas inflows.

The increase in the SFR is also reflected in the  $\alpha$ -enhancement,  $[\text{O}/\text{Fe}]$ , of the gas in the central region (dotted line of Fig. 2d). This central  $\alpha$ -enhancement is present from the first pericentre, but is much stronger around the second one. Note that the infalling gas into the central region is low  $\alpha$ -enhanced as expected in a disc galaxy such as that of the Milky Way (solid line of Fig. 2d), indicating that the increase of oxygen in the central region is principally due to SN II associated with the central starburst. These general results are in agreement with those reported by Montuori et al. (2010), although these authors did not consider chemical enrichment self-consistently. As we will discuss in the following section, our simulations allow us to make further advances on this issue.

Previous works (e.g. Barnes & Hernquist 1996; Cox et al. 2008; Di Matteo et al. 2008; Hopkins et al. 2009) have already reported how SF histories of interacting systems depend on the initial conditions and orbital parameters. Hence, the trends shown in Fig. 2 for SimI might vary among the analysed simulations as we will discuss in the following sections.

### 3.1 Could the $\alpha$ -enhancement clock the interaction?

As already shown for SimI, the  $\alpha$ -enhancement starts to be detected after the first close passage. However, the most significant increase is recorded after the second one. In order to analyse if the  $\alpha$ -enhancement could be used to time the interaction as suggested by Montuori et al. (2010), we study the ISM enrichment history along the interactions and its dependence on different orbital configurations.

Fig. 3 shows the evolution of  $[\text{O}/\text{Fe}]$  in the central regions for different simulations with different orbital parameters: SimI, SimII and

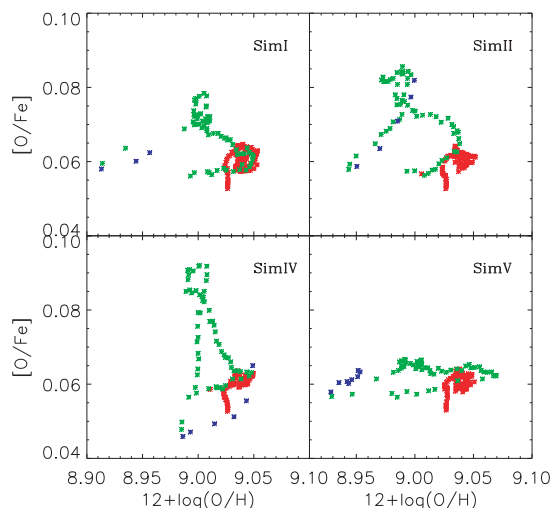


**Figure 3.** Evolution of central abundances as the galaxy's interaction proceeds for different simulations: I, II, IV and V. Red symbols identify the phase of interaction before the first pericentre, green points identify the phase between the first and second pericentres and blue ones identify the final merging phase after the second pericentre.

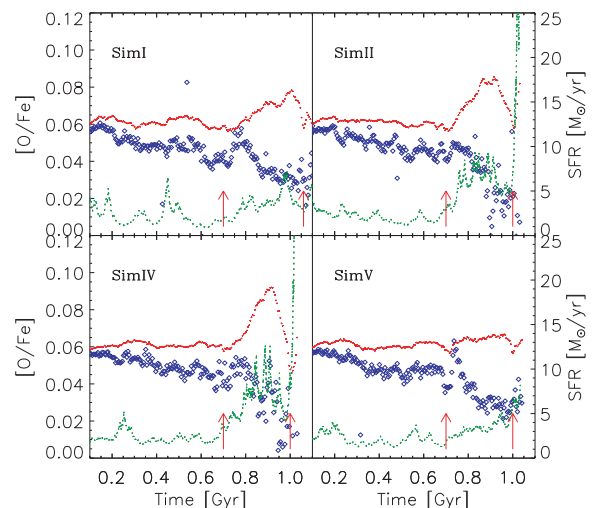


**Figure 4.** Evolution of  $\alpha$ -enhancement of the central region (red dotted lines) and of the infalling gas (blue open symbols) and the SFR (green lines) for different simulations: I, II, IV and V. Arrows in each panel indicate the first and second pericentres.

SimV. We also include SimIV which assumes a lower energy per SN event, but otherwise has the same parameters as SimII. We find that before the first close passage (red points), the different simulations neither exhibit any significant variations in the  $12 + \log(\text{O}/\text{H})$  nor  $[\text{O}/\text{Fe}]$  values. However, different feedback parameters and orbital configurations impact differently on the ISM chemical enrichment during the interacting phase between the first two pericentres (green points). As a general result, we find an increase in the  $[\text{O}/\text{Fe}]$ , except for the coplanar retrograde orbit (SimV).

In order to understand these differences in the  $\alpha$ -enhancement, Fig. 4 shows the central  $\alpha$ -enhancement and the SFR for one of the interacting galaxies in each simulation. As expected, the central  $\alpha$ -enhancement (red dotted lines) correlates with the SF activity (green lines). We find that between the first and the second pericentres, the  $[\text{O}/\text{Fe}]$  reaches the highest values for coplanar direct orbits (SimII and SimIV), decreases as inclination increases (SimI) and is almost negligible for the coplanar retrograde interaction (SimV). Note that in agreement with previous results by Di Matteo et al. (2007), we find that coplanar direct interactions trigger stronger starbursts than coplanar retrograde configurations during the pre-merger phase (see fig. 8 of their paper). We also find that the simulation with standard feedback (SimII) has slightly lower levels of the  $[\text{O}/\text{Fe}]$  and SFR than the case of low-energy feedback (SimIV) because in the later, SN feedback drives weaker galactic outflows, being less efficient at transporting material out of the central regions.

As discussed previously by Montuori et al. (2010), the  $\alpha$ -enhancement observed in interacting galaxies before the final coalescence of systems might date the interaction. However, we find that this is valid when the  $\alpha$ -enhancement is only regulated by the SF process. In this case, the increase in  $[\text{O}/\text{Fe}]$  during the interacting phase would indicate the occurrence of a recent starburst (approximately  $< 1$  Gyr) because the ISM has not had enough time to be heavily enriched by SN Ia yet. On the contrary, the detection of a decreasing  $[\text{O}/\text{Fe}]$  value would indicate that SN Ia had time to release Fe into the ISM, which means that the time elapsed since the last starburst is longer than approximately  $\sim 1$  Gyr. Our simulations which follow the dynamical and chemical evolution along the interaction suggest that other factors are also involved in the regulation of the  $\alpha$ -enhancement. As can be seen for SimI, SimII

and SimIV (Fig. 4), the increase in the  $\alpha$ -enhancement after the first pericentre is followed by a drop before the second pericentre. We find that this dilution of the central  $\alpha$ -enhancement is caused by the low  $[O/Fe]$  enhancement of the very important gas inflow (open blue symbols in Fig. 4), triggered during the second close approach of the galaxies. This gas inflow vanishes the clear traces in the central abundances left by the SF activity, restarting the clock to date the interaction.

Hence, our simulations suggest that the  $\alpha$ -enhancement can only indicate the proximity to the first pericentre, providing extra information on the parameters of the encounter since those with orbits close to coplanar retrograde configurations would tend to have very mild enhancement (SimV in Fig. 4). However, our findings also suggest that the chance to observe close galaxy pairs with central  $\alpha$ -enhancement might be low because of the short time interval

over which it could be detected (less than approximately 0.2 Gyr according to our experiments).

### 3.2 Gas-phase metallicity profiles of wet low-redshift interactions

As shown in the previous section, galaxy–galaxy interactions have a clear effect on the central abundances and the SF of wet interacting systems at low redshift caused by the dynamical perturbation induced on the gas component. In order to illustrate how this affects the gas-phase metallicity profiles, we show a sequence of oxygen abundance maps which plot the spatial distribution for the interacting galaxies of SimI at a different stage of the interaction, with their corresponding oxygen abundance profiles (Fig. 5). It can be appreciated how the metallicity profile changes as the interacting

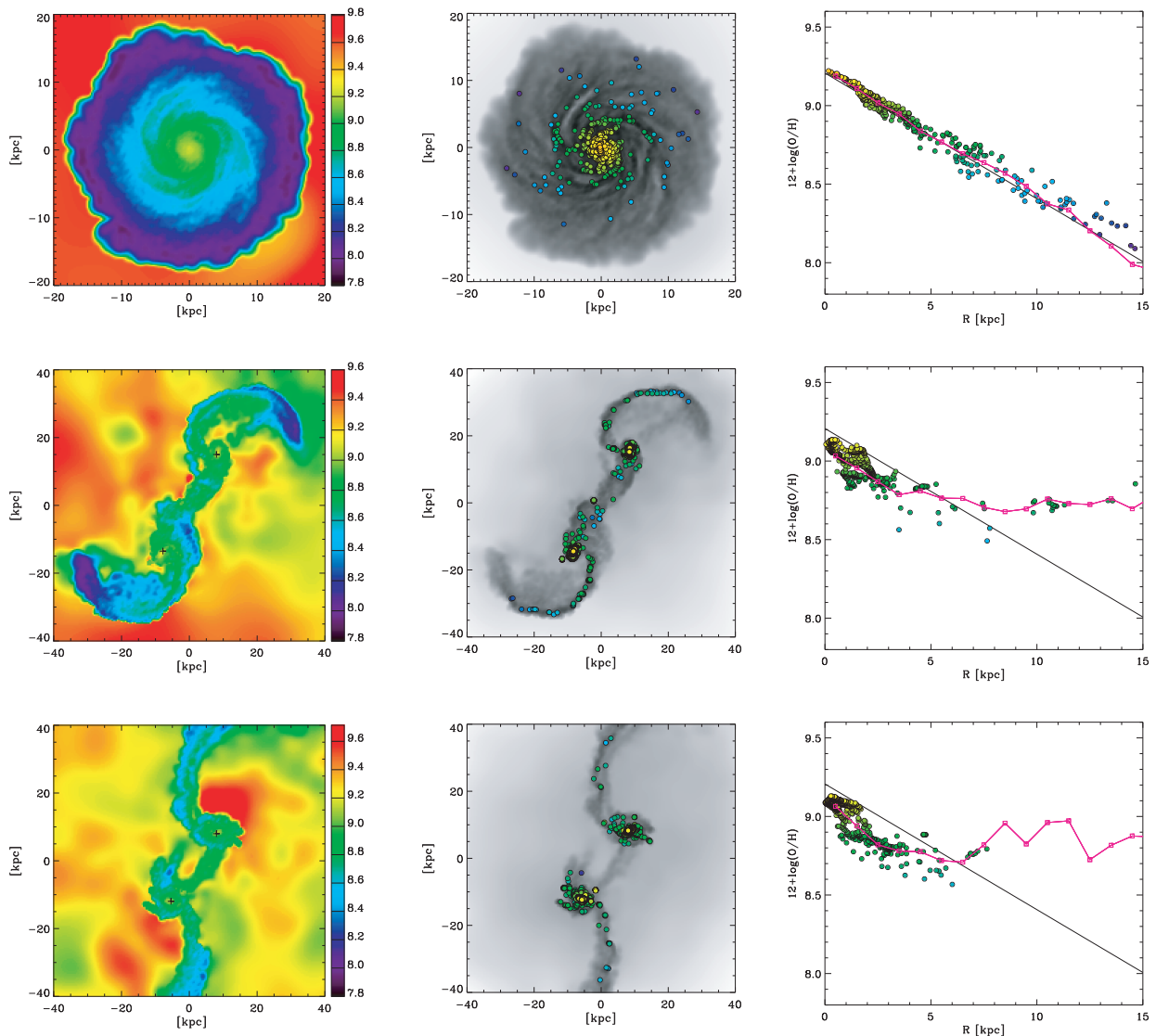


**Figure 5.** Time sequence of the chemical properties in the gas component of SimII (before the first pericentre at  $t = 0.3$  Gyr (upper panel), after the first pericentre at  $t = 0.8$  Gyr (middle panel) and just before the second pericentre at  $t = 0.9$  Gyr (lower panel)). Left-hand panels: oxygen abundance maps. Middle panels: gas density map (in grey) and oxygen abundances of the star-forming regions (colour circles are colour-coded as the left-hand panels). Right-hand panels: gas-phase oxygen abundance profiles. The black line shows the initial metallicity gradient. The magenta line and symbols show the gas-phase metallicity gradient computed with all the gaseous particles. For the top panels, only one galaxy is shown since the two galaxies are very distant and the field of view is smaller than the bottom panels. The right-hand panels show that the abundance gradients computed by radial binning of all the gaseous particles are in good agreements with the gradients determined with only the abundances of star-forming regions, as is done with observations.

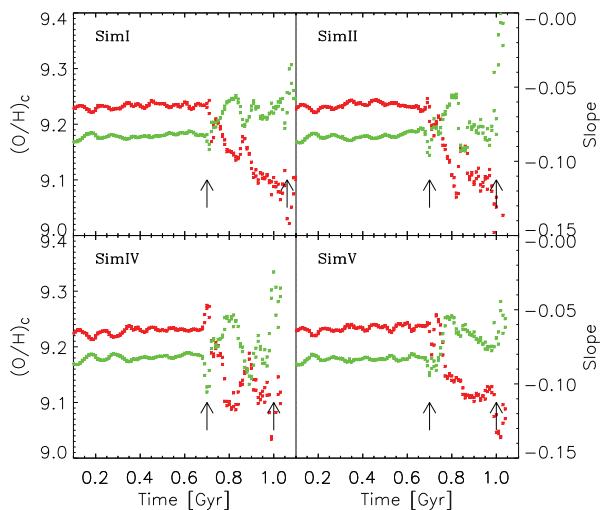


**Figure 6.** Evolution of the linear regression coefficients ( $(O/H)_c$ : red and slope: green) of the oxygen abundance radial profile, computed in a range of  $3\epsilon_G$ –7 kpc for different simulations: I, II, IV and V. Arrows indicate the first and second pericentres.

system gets closer. This evolution is mainly related to the flattening of the profile caused by a decrease in central metallicities and a simultaneous increase in the abundances in the external region of the disc. We also show in Fig. 5 (right-hand panel) that the abundance gradients computed by radial binning of all the gaseous particles are in good agreement with the gradients determined with only the abundances of star-forming regions, as is done with observations.

### 3.2.1 Internal oxygen abundance profiles

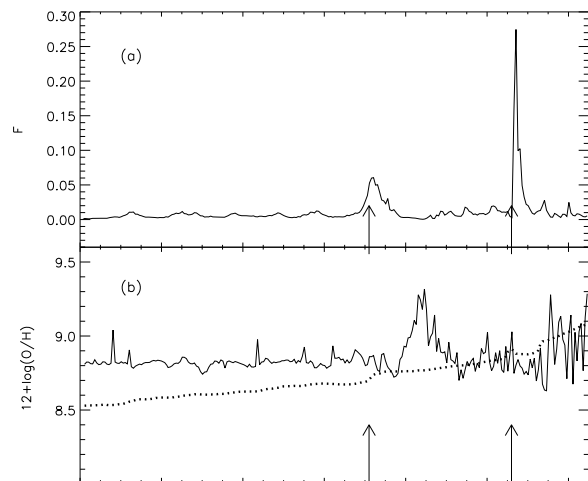
In order to quantify the evolution of internal metallicity profiles, we carry out a linear regression fit to estimate the central oxygen abundances,  $(O/H)_c$ , and slopes. The internal profiles are defined in the range of  $3\epsilon_G$ –7 kpc. The inner radial limit corresponds to three times the gravitational softening used for baryons, and for the external radius,  $R_{\text{ext}} = 7$  kpc corresponds to approximately three scalelengths of the initial stellar disc.

Fig. 6 shows the linear-fitting coefficients of the radial profiles for different simulations. As can be appreciated, there is a significant evolution of internal profiles after the first pericentre, which is consistent with a central dilution of abundances as expected from the discussion of the previous subsection. In agreement with observations (Kewley et al. 2006; Rupke et al. 2008) and previous numerical works (Rupke et al. 2010a), the drop in  $(O/H)_c$  is about 0.2 dex (red points). We also find that the final metallicity gradients are flatter than those in earlier stages of the interaction (green points) in agreement with Kewley et al. (2010) and Rupke, Kewley & Chien (2010, and references therein).

Note that although the evolution of internal profiles seems to be not very sensitive to different orbital configurations in wet major mergers at low redshift, our results show some evidence that galaxies in coplanar direct orbits (SimII and SimIV of Fig. 6) experience a larger flattening than those in coplanar retrograde ones (SimV of Fig. 6).

### 3.2.2 External oxygen abundance profiles

As mentioned above, the external abundance profiles rise as the galaxy interaction proceeds. This is a common feature to all simulations; hence, we will take SimI again for illustration purposes.



**Figure 7.** (a) Fraction of gas getting into the external region ( $R > R_{\text{ext}} = 7$  kpc) as a function of time. (b) Oxygen abundance of the gas getting into this external region (solid line) and the mean external abundances (dotted line) as a function of time. Arrows indicate the first and second pericentres. These calculations are shown for one galaxy member of SimI as an example.

We define the external region of the gaseous disc as everything outside  $R_{\text{ext}} = 7$  kpc, which also denotes quite well the radius where the outer profiles depart from that defined by the central region (Fig. 5). Then, we estimate the fraction of gas which has gotten into the external disc between two available time intervals, as well as the metallicity of this gas as a function of time.

As can be seen from Fig. 7(a), close to each pericentre, the external disc of interacting systems receives a significant fraction of gas, principally close to the second one ( $\sim 30$  per cent at the second pericentre). This gas comes from the inner regions of the disc as the arms get opened and distorted by tidal forces (Fig. 5). As a consequence, this gas tends to have high oxygen abundances (Fig. 7b, solid line), which partially contribute, after the first pericentre, to increase the mean external abundances by  $\approx 0.4$  dex (Fig. 7b, dotted line). This result is in agreement with Rupke et al. (2010), who find that tidal tails transport metal-enriched gas from the galaxy’s inner regions to the outskirts.

On the other hand, there is new SF activity triggered in the external regions, on the spiral arms as can be seen from Fig. 5. These new stars will also contribute with new SN II to the enrichment of the external ISM. Therefore, the evolution of the external abundances is produced by the combined effects of these two processes: (i) the *in situ* SF activity and (ii) the gas-rich material coming from inner regions as the interaction takes place and the spiral arms get distorted.

## 4 METALLICITY EVOLUTION IN WET HIGH-REDSHIFT MERGERS

In previous sections, we have analysed wet low-redshift interactions of galaxies with around 20 per cent of the disc in the form of gas. Here, we will discuss the metallicity evolution in interacting systems when the initial amount of gas is increased up to 50 per cent (SimVI). This scenario is suitable for studying wet galaxy encounters at high redshift.

For this simulation, we have chosen the same orbital configuration of SimII, but with a modified initial distribution of baryons in order to start with more gas-rich systems (cf. Table 1). We have also adopted the same SF and SN parameters as for SimII. The

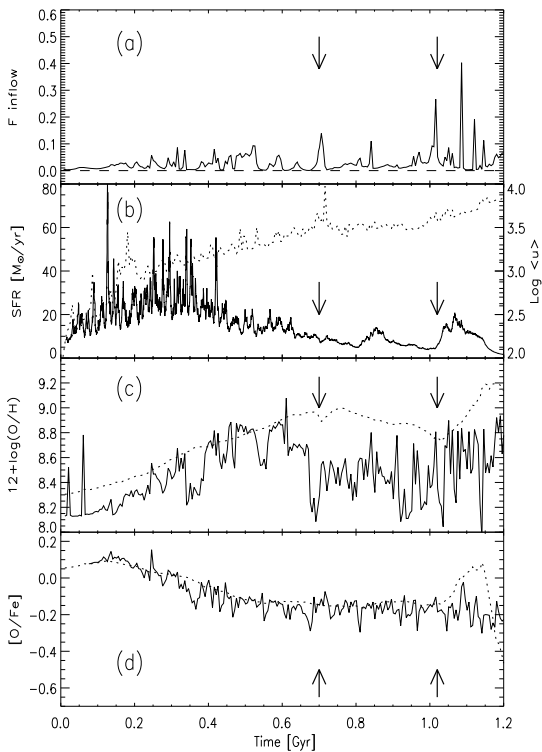


**Figure 8.** High gas-rich simulation (SimVI): (a) Fraction of gas inflowing within  $R_{\text{cen}}$  as a function of time. (b) Evolution of the SFR (solid line) and of the mean internal energy ( $u$ ) of the gas (dotted line). (c) Oxygen abundance of the infalling gas (solid line) and the mean central oxygen abundance (dotted line), computed within  $R_{\text{cen}}$ . (d)  $\alpha$ -enhancement of the infalling gas (solid line) and its mean central value (dotted line). Arrows indicate the location of first and second pericentres.

initial abundance gradient has been adjusted to be consistent with the observations of the mass–metallicity relation at high redshift. Particularly, we used the observations of Maiolino et al. (2008) at  $z \sim 3.5$ . Hence, the initial zero-point is lower and the gradient is steeper than in the case of less gas-rich interactions (see Section 2).

Fig. 8(a) shows the gas inflows for one of the galaxy members in SimVI. In this case, the amount of gas that falls into the central region is more significant than in its less gas-rich counterpart throughout the whole simulated time interval. Particularly, after the second pericentre, the gas inflow roughly duplicates that of the less gas-rich interacting galaxies.

The comparison of the SFR evolution of more gas-rich galaxies (Fig. 8b) with that of their less gas-rich counterparts (Fig. 2c) shows that long before the first close passage, the SFR of the more gas-rich system is more active (around  $30 M_{\odot} \text{ yr}^{-1}$ ) than that of their less gas-rich counterpart. This is mainly due to the higher fraction of gas available for SF. Previous works (Bournaud, Elmegreen & Elmegreen 2007; Bournaud et al. 2008) have suggested that gas-rich galaxies might experience greater instability on the gaseous disc, which can lead to an intense SF activity via fragmentation and clump formation. In order to check this behaviour in our simulations, we compare the evolution of gaseous discs for galaxies in SimI and SimVI. Fig. 9 shows projected gas distributions of one member of the interacting system in SimI (upper panels) and in SimVI (lower panels), computed for different snapshots during the interaction. From these figures it is clear that, while the gaseous disc in the less gas-rich simulation evolves more smoothly, in the more gas-rich system it has highly fragmented and formed high-density clumps

where the gas satisfies the condition to form stars in agreement with previous works<sup>2</sup>. We checked that the Jeans mass is resolved by at least four gas particles so that fragmentation can be numerically described. As can be appreciated in the first low panel, the more gas-rich system shows a high level of disc fragmentation well before the first close passage at 0.3 Gyr, when the two interacting galaxies are separated by more than 100 kpc and consistent with the peak in the SFR (see Fig. 8b). This suggests that the internal fragmentation of gas-rich discs is principally driven by their own self-gravity. To prove that this early strong SF activity is not induced by the interaction, we run an isolated galaxy case with the same SF and SN parameters. The clump formation is also present in our isolated galaxy run. Previous works have shown that galaxy interactions reinforce the level of disc fragmentation for mergers at low and high redshifts (Teyssier, Chapon & Bournaud 2010; Bournaud et al. 2011, respectively). The detailed analysis of this issue will be part of a future paper focused on clump formation in isolated and interacting disc galaxies.

After the intense SF activity reported during the early stage of interaction, the SFR in the more gas-rich galaxies begins to decline with two subsequent maxima shortly after the first and second pericentres, respectively (Fig. 8b). The induced SF activity during the close encounters is less important than that expected considering the strong gas inflows experienced by these galaxies at these stages of evolution (Fig. 8a). We investigate which mechanism could be operating against the triggering action of gas inflows to inhibit the SF activity. We analysed the thermodynamical properties of the gas, finding that its internal energy (dotted line of Fig. 8b) increases continuously fed by the SN feedback. This process is responsible for heating up and blowing away an important fraction of gas with an increasing efficiency as the galaxy approaches the second pericentre when it loses  $\sim 60$  per cent of its initial gas mass ( $\sim 10$  per cent is lost at the first pericentre and more than 80 per cent at the merging phase). As a consequence, the level of SF activity is not only directly correlated with the strength of the gas inflows, but it is also modulated by the SN feedback which is, in this simulation, more important than in the less gas-rich interactions because of the larger amount of available gas to feed SF.

We investigate the chemical evolution of the ISM by analysing the O/H abundances and  $\alpha$ -enhancements as in the less gas-rich interactions. Fig. 8(c) shows the evolution of oxygen abundance of the infalling gas and of the central region. From this figure, we can see that the central metallicity of the gas increases steadily up to the first pericentre. We can also appreciate that the gas inflows, driven into the central regions during the first main starburst, are increasingly oxygen-rich as a consequence of the on-going important SF activity. This is a consequence of the first early starburst which is not present in less gas-rich interactions. However, from the first to the second pericentre, the low metallicity of the infalling gas produces the oxygen dilution of the central region just as in wet local interactions (Fig. 2b). The different levels of enrichment of these gas inflows are due to their different origins: high-metallicity inflows involved gas located nearby the central region, while lower metallicity inflows come from more external ones. Since our discs have initially metallicity gradients, these different origins imply

<sup>2</sup> Our less gas-rich simulation also shows clumps along the disc but with a significant lower level of fragmentation than in the more gas-rich counterpart. The contribution of these clumps to the SF activity in the less gas-rich mergers and a comparison with observations will be carried out in a future paper.

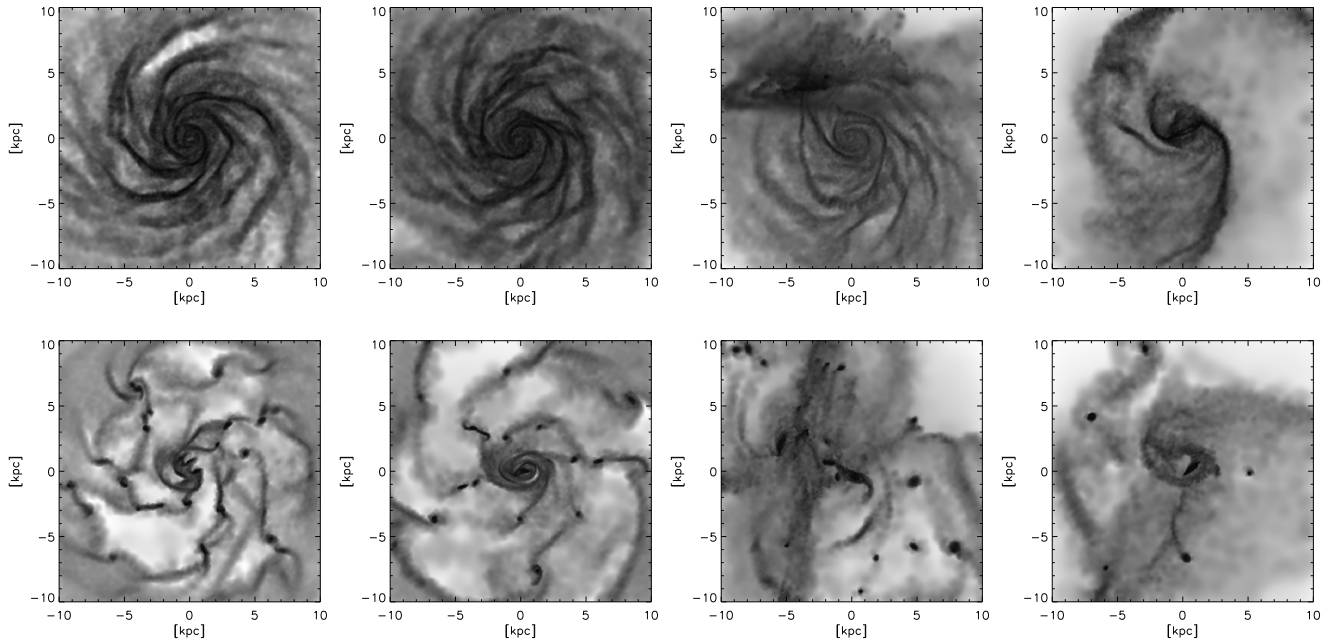


**Figure 9.** Projected gas mass distribution on to the disc plane of one interacting galaxy for the less gas-rich simulation SimI (upper panels) and for its more gas-rich counterpart SimVI (bottom panels). Gas density maps are shown from the left to the right: at 0.3 Gyr when the galaxies are separated by  $\approx 100$  kpc, well before the first pericentre; at 0.45 Gyr just at the first pericentre at 0.7 Gyr; and at 0.8 Gyr between the first and second pericentres.

different levels of enrichment. To visualize this, in Fig. 10 (upper panel) we show the minimum, maximum and the median locations on the disc plane of those gas particles which will be immediately incorporated into the gas inflows<sup>3</sup>. Before the first pericentre most of the gas that falls into the central regions comes from about 4.5 kpc and hence is principally driven by internal dynamics, while during the interactions the tidally driven gas inflows are able to transport material inward from further away regions of the disc as can be seen in Fig. 10 (upper panel).

In Fig. 10 (lower panel), we show the stellar age gradients as a function of time. We can see sharp drops in the profiles as signatures of a discontinuous SF distribution along the disc, reflecting the clumpy SF activity. Profiles in blue, red and green show the evolution of the SF distribution before the first pericentre. As shown by these profiles, the strong SF activity reported during this period (Fig. 8b) is located not only in the central region but also extended in the outskirts of the galaxy, contributing to enrich the ISM. As the interaction goes on, the main SF activity takes place principally in the central regions which gets rejuvenated.

As a consequence of the contribution of a low-metallicity gas inflows during the close interaction (between the two first pericentres) the central O/H abundance decreases by  $\approx 0.4$  dex (Fig. 8c, dotted line). The fact that the central oxygen abundance decreases more slowly than that of the infalling gas, at this stage of the interaction, is a consequence of the SF activity being more concentrated in the central region, continuously supplying new chemical elements via SN II events. After the second pericentre, we observe a second SFR enhancement driven by new gas inflow (Figs 8a and b). This SF activity is very centralized in the nuclear region of the galaxy as shown in Fig. 10 (lower panel), increasing the central O/H abundance (Fig. 8c, dotted line).

<sup>3</sup> The location is determined as the distance of a given particle to the centre of mass just before it moves into the central region,  $R < R_{\text{cen}}$ .

Finally, we also investigate the  $\alpha$ -enhancement of wet encounters at high redshift. Fig. 8(d) shows that the initial [O/Fe] value is consistent with the  $\alpha$ -enhancement observed in less gas-rich interactions (Fig. 2d). The subsequent evolution of the  $\alpha$ -enhancement shows that immediately after the second pericentre and simultaneously to the SFR enhancement, the central [O/Fe] (Fig. 8d, dotted line) exhibits a sharp increase produced by an important increase of SN II feedback associated with the more active central SF. After this  $\alpha$ -enhancement, we find a significant drop in the central [O/Fe] values of around 0.8 dex. This drop is caused by the injection of Fe elements into the ISM by SNIa, whose progenitors formed  $\sim 1$  Gyr before, during the main starbursts.

#### 4.1 Oxygen abundance profiles of wet interactions at high redshift

In this section, we will quantify the effect of wet interactions at high redshift on the gas-phase metallicity profiles. Similarly to the case of wet interactions in the local Universe, the evolution of metallicity profiles in the more gas-rich interacting galaxies shows a clear flattening and the central dilution of O/H abundances. We quantify the evolution of the metallicity profiles by performing linear regressions. Fig. 11 shows the  $(\text{O}/\text{H})_{\text{C}}$  and slopes as a function of time (red and green points, respectively).

As expected, we find that the evolution of  $(\text{O}/\text{H})_{\text{C}}$  matches that of the central abundances computed within  $R_{\text{cen}}$  (see the dotted line in Fig. 8c). We can see an increase of around 0.6 dex in the  $(\text{O}/\text{H})_{\text{C}}$  during the approaching phase, while after the first pericentre, the decrease reflects the impact of the low-metallicity inflows driven by the interactions. These low-metallicity inflows produce a decrease of  $\approx 0.5$  dex in the oxygen central abundance, while in less gas-rich counterparts, the decrease is of  $\approx 0.2$  dex towards the final merging stage (Fig. 6).

The evolution of the gradients shows an approximately constant slope until the first pericentre where the profiles get more negative



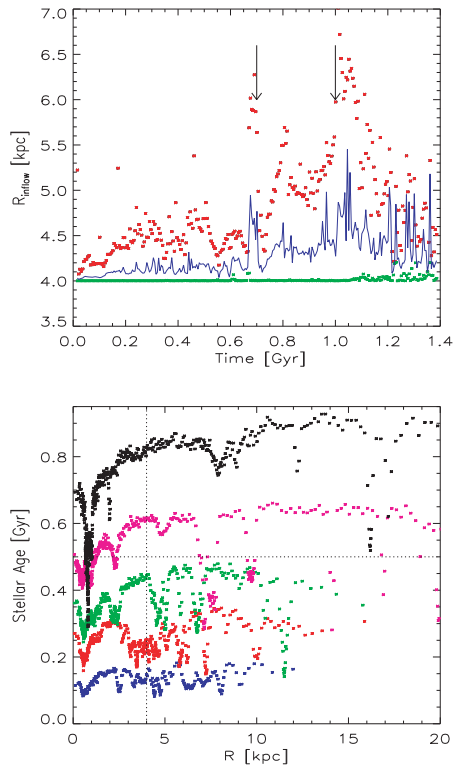


**Figure 10.** Upper panel: minimum (green), median (blue solid line) and maximum (red points) location of gas particles that will be immediately incorporated into the gas inflow in the more gas-rich simulation (SimVI). Arrows indicate the location of first and second pericentres. Lower panel: stellar age profiles for different stages of evolution of SimVI, corresponding to 0.3 Gyr (blue), 0.5 Gyr (red), 0.66 Gyr (green, first pericentre), 0.86 Gyr (magenta, after the first pericentre) and 1.16 Gyr (black, second pericentre). The vertical line indicates  $R_{\text{cen}}$ .

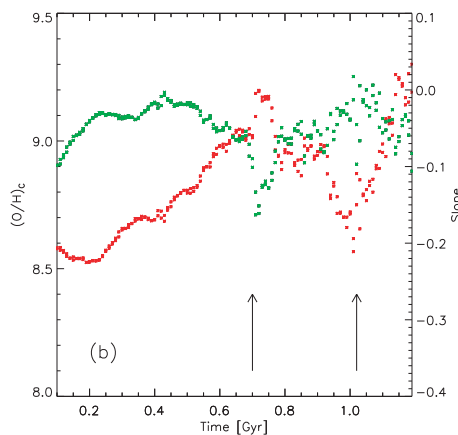


**Figure 11.** Evolution of the linear regression coefficients ( $(\text{O}/\text{H})_{\text{C}}$ : red and slope: green) of the oxygen abundance profiles in the more gas-rich encounter (SimVI) computed in a range of  $3\epsilon_{\text{G}}-7$  kpc. Arrows indicate the first and second pericentres.

as a result of the oxygen carried into the central region by the early metal-rich inflows. However, from the first pericentre there is a continuous mean flattening of the metallicity profiles which gets even slightly positive around the second pericentre where again it

starts to get steeper towards more negative values as more oxygen is pumped in by SN II produced during the second tidally induced starburst (see Fig. 8b).

## 5 DISCUSSION

Several interesting aspects remain to be understood or even acknowledged in galaxy interactions and their impact on chemical properties. Numerical simulations are, indeed, the most suitable tool to study them. Different authors with different techniques and levels of complexity have made important contributions (e.g. Perez et al. 2006; Montuori et al. 2010; Rupke et al. 2010a) to this area over the last years. All works agree to show the central abundance dilution due to low-metallicity inflows triggered during the interaction.

Our simulations allow us to contribute further to explore the role played by the induced SF and SN feedback in modulating the strength of this metallicity dilution and the evolution of the metallicity gradients. Particularly, we run SimIII which only follows the dynamics of the gas with fixed metallicity assigned according to an initial abundance profile. No new SF activity is permitted in SimIII. As can be appreciated by comparing the evolution of the central oxygen abundances in SimII and SimIII in Fig. 12, neglecting the subsequent SF and chemical enrichment leads to an overestimation of the metallicity dilution (and flattening of the gradients).

One of the effects of SF is the generation of new SN II which contributes with new chemical elements and also pumps energy into the ISM. The strongest the gas inflows, the strongest the starbursts and consequently, the impact of SN feedback which can heat up and blow away significant fractions of the remaining enriched gas, regulating the subsequent SF activity and modulating the chemical enrichment. In SimIV, we use a lower energy input for SN event and thus, reducing the impact of energy feedback. As a consequence, a more intense SF can develop producing a higher chemical enrichment than in SimII. From Fig. 12, we can see that the central oxygen abundance is very similar to that of SimII until the first pericentre, while after that the mean oxygen abundance in SimIV is larger since the impact of the mass-loaded outflows is weaker and is not so efficient at transporting material outside the central region and at inhibiting the SF activity (the effects on the SFR,  $\alpha$ -enhancement and metallicity profiles can be visualized comparing results from SimII and SimIV in Figs 3, 4 and 6). Hence, it is important to model the ongoing SF activity in a self-consistent way with energy and

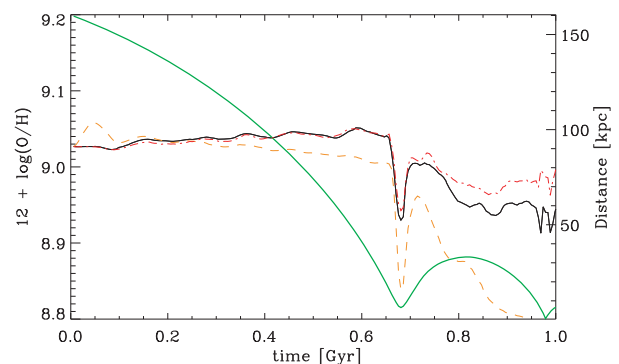


**Figure 12.** Effect of SF and feedback: evolution of central gas-phase oxygen abundances ( $R < R_{\text{cen}}$ ) of one galaxy in SimII (black full line), SimIII (orange dashed line) and SimIV (red dash-dotted line). The relative distance between the centre of mass of the simulated galaxies is also plotted (green line).

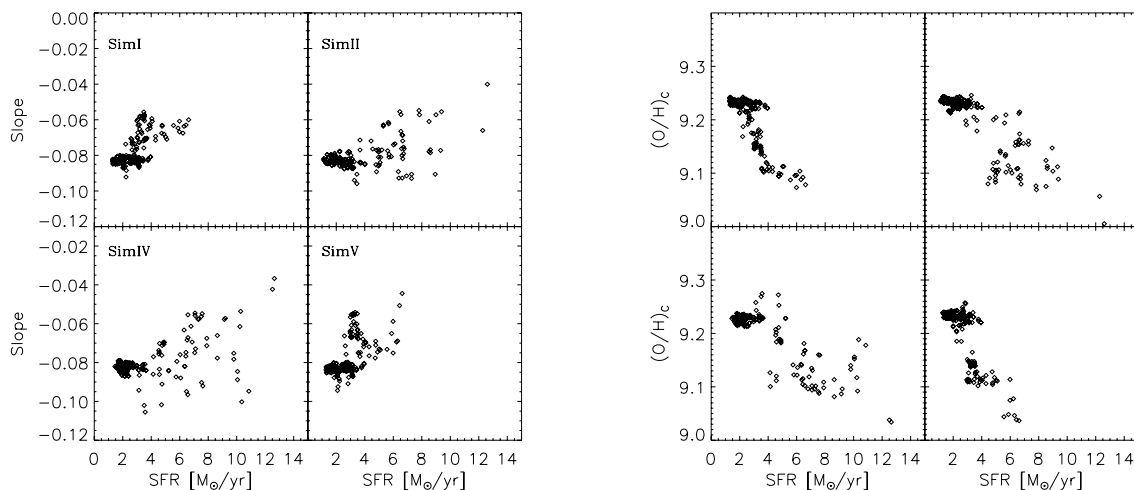


**Figure 13.** Metallicity gradients and central abundances as a function of the SFR for interacting galaxies in SimI, SimII, SimIV and SimV.

chemical SN feedback in order to have a more comprehensive picture of the evolution of the metallicity and gradients during galaxy interactions.

As a consequence of this complex interplay of various physical processes, we find that some a priori obvious correlations are actually difficult to detect. One example of this is the use of  $\alpha$ -enhancement to clock the interaction as we have already discussed in Section 3.1. Another expected correlation is that between the strength of the central starbursts and the metallicity dilution. In Fig. 13, we plot the slopes of the metallicity gradients and the central oxygen abundances as a function of the SFR for wet low-redshift interactions. We can see that globally there is a correlation so that the highest the SFR is, the strongest is the metallicity dilution and the shallower the abundance profiles. However, the relations depend strongly on the orbital parameters. SimI and SimV have weaker starbursts than SimII, but nevertheless they experienced metallicity dilution in the central regions due to the tidally induced gas inflows. Hence, according to our findings, it might be difficult to establish this correlation observationally where galaxy pairs can be observed at different stages of evolution and with a variety of orbital parameters.

Regarding the gas richness, from Fig. 11 we can see that, although there is a global trend in diluting central metallicity and in flattening the mean gradients, there are also fluctuations which correlate with the triggering of inflows and the injection of fresh oxygen by the new SN II. Nevertheless, the mean metallicity dilution is stronger than the less gas-rich counterpart (Fig. 6). Hence, the gas richness is another key factor.

Depending on the astrophysical properties and orbital parameters, galaxies in pairs can be located differently on the mean mass–metallicity relation depending on the stage of the interaction at which they are observed. This effect might be particularly relevant for the study of high-redshift galaxies and could be at the origin of the apparent increase with the redshift of the scatter in the mass–metallicity relation. It could also explain the presence of outliers in the local mass–metallicity relation. For example, more gas-rich systems observed, just as they are first approaching, might be dominated by the massively and clumpy SF activity taking place at all radii, before the interaction can actually trigger larger scale inflows capable of transporting low-metallicity gas into the central region. Hence, these galaxies might show an excess of oxygen (e.g. Michel-Dansac et al. 2008).

## 6 CONCLUSION

By using hydrodynamical simulations of interacting pre-prepared galaxies of comparable masses, we study the chemical evolution of the ISM during the interactions. Our simulations include self-consistently, SN feedback and a detailed chemical model, which allow us to follow the evolution of the gas-phase metallicity from the initial to the final stages of an interaction. These simulations constitute a unique set to study the effects of interactions on chemical properties.

We analyse the different chemical response to galaxy interactions, varying orbital configurations, strength of energy SN feedback and initial gas fractions in the galaxy discs. Particularly, we focused our study on wet interactions in the local Universe. For comparison, we also analysed a more gas-rich interaction in order to reproduce wet mergers typical of high redshift.

Our main results can be summarized as follows.

(1) We find that a low-metallicity gas inflow developed from the first close passage dilutes the central oxygen abundance and triggers starbursts at the first and second pericentres. We find that the amplitude of the central oxygen dilution of close galaxy pairs is fairly consistent with observations. This dilution is observed with a large scatter for interacting systems separated by less than 30 kpc. The amplitude varies according to orbital configurations and phases of interactions.

During the interactions the metallicity gradients get quite shallower with fluctuations, such as sometimes they are a slightly positive gradient. Both the release of new chemical elements and energy by SN II, produced during the tidally induced starburst, modulate the strength of the central dilution and the metallicity gradients. This behaviour seems to be in good agreement with what is observed for galaxy pairs (observations by Kewley et al. 2006, 2010). We note that it is not possible from these simulations to test the claims of Cresci et al. (2010) since our boundary conditions are not consistent with a cosmological scenario where gas accretion from the intergalactic medium can fuel the galaxies.

(2) We find an increase in the interstellar [O/Fe] values, observed after the first pericentre as suggested by previous works. This  $\alpha$ -enhancement does not only reflect the tidally induced SF activity but is also affected by galactic outflows and the abundances of the gas inflows. As a consequence, we show that the  $\alpha$ -enhancement can only indicate the proximity to the first pericentre and in those

encounters with non-coplanar retrograde orbits. After the first pericentre, gas inflows might dilute the central [O/Fe] values, erasing the trace left by the SF activity and restarting the clock to date the interaction. We also note that the period of time where this enhancement could be observed is quite short ( $<0.2$  Gyr).

(3) More gas-rich interactions show massive and clumpy SF on the disc from early stages of the interaction. During the interaction, from the first pericentre to the final stages, we find similar behaviours as in the case of the less gas-rich runs with the particularities imprinted by the more gas availability. Gas richness has an impact on the strength of low-metallicity gas inflows which in the simulated interaction are able to dilute the central abundances by 0.5 dex, a factor of 2.5 larger than in its less gas-rich counterpart. There are important variations in the central abundances and gradients as the interaction of more gas-rich galaxies proceeds due to the competition between various processes, such as the injection of new chemical elements after starbursts, the action of outflows which blow away part of the enriched material and the gas dynamics of clumpy discs.

(4) We find a correlation between the metallicity gradient, the central chemical abundance and the strength of the SF activity. However, the slope and scatter of these correlations depend on orbital parameters, SN outflows and gas richness. Hence, it is not a simple relation which can be easily unveiled observationally. The metallicity gradients are affected by the strength of the central nuclear starbursts and the extended SF detected in the outer regions of the galaxies. Star formation in clumps is also found to play a role in modulating the metallicity gradients. A detailed analysis of disc fragmentation as a function of gas richness will be carried out in a forthcoming paper.

Our results suggest that metallicity evolution is closely related to gas dynamics during the encounters. Denying processes, which affect the gas dynamics and its level of enrichment such as SF and SN feedback, can contribute either to overestimate or underestimate the effects on the central abundance dilution or metallicity gradients. These findings show that there are still many issues to be addressed in galaxy interactions and their role in chemical evolution.

## ACKNOWLEDGMENTS

We thank the referee, F. Bournaud, for a constructive report. PBT thanks ISIMA 2010 for the hospitality and challenging environment which allowed part of this work to be done. This work was partially supported by the Consejo Nacional de Investigaciones Científicas y Técnicas (PIP 2009/0305), Agencia Nacional de Promoción Científica y Técnica [PICT 32342 (2005)], Max Planck 245 (2006), the Agence Nationale de la Recherche (ANR-08-BLAN-0274-01).

## REFERENCES

Alonso M. S., Lambas D. G., Tissera P., Coldwell G., 2006, *MNRAS*, 367, 1029  
 Barnes J., Hernquist L., 1996, *ApJ*, 471, 115  
 Barton E. J., Geller M. J., Kenyon S. J., 2000, *ApJ*, 530, 660  
 Bournaud F., Elmegreen B. G., Elmegreen D. M., 2007, *ApJ*, 670, 237  
 Bournaud F. et al., 2008, *A&A*, 486, 741  
 Bournaud F. et al., 2011, *ApJ*, 730, 4  
 Cox T. J., Jonsson P., Somerville R. S., Primack J. R., Dekel A., 2008, *MNRAS*, 384, 386

Cresci G., Mannucci F., Maiolino R., Marconi A., Gnerucci A., Magrini L., 2010, *Nat*, 467, 811  
 De Rossi M. E., Tissera P. B., Pedrosa S., 2010, *A&A*, 519, 89  
 Di Matteo P., Combes F., Melchior A.-L., Semelin B., 2007, *A&A*, 468, 61  
 Di Matteo P., Bournaud F., Martig M., Combes F., Melchior A.-L., Semelin B., 2008, *A&A*, 492, 31  
 Dutil Y., Roy J.-R., 1999, *ApJ*, 516, 62  
 Ellison S. L., Patton D. R., Simard L., McConnachie A. W., 2008, *AJ*, 135, 1877  
 Ellison S. L., Patton D. R., Simard L., McConnachie A. W., Baldry I. K., Mendel J. T., 2010, *MNRAS*, 407, 1514  
 Hopkins P. F., Cox T. J., Younger J. D., Hernquist L., 2009, *ApJ*, 691, 1168  
 Kewley L. J., Geller M. J., Barton E. J., 2006, *AJ*, 131, 2004  
 Kewley L. J., Rupke D., Jabran Zahid H., Geller M. J., Barton E. J., 2010, *ApJ*, 721, L48  
 Khochfar S., Burkert A., 2006, *A&A*, 445, 403  
 Lambas D. G., Tissera P. B., Alonso M. S., Coldwell G., 2003, *MNRAS*, 346, 1189  
 Maiolino R. et al., 2008, *A&A*, 488, 463  
 Michel-Dansac L., Lambas D. G., Alonso M. S., Tissera P., 2008, *MNRAS*, 386, L82  
 Mihos J. C., Hernquist L., 1996, *ApJ*, 464, 641  
 Montuori M., Di Matteo P., Lehnert M. D., Combes F., Semelin B., 2010, *A&A*, 518, A56  
 Mosconi M. B., Tissera P. B., Lambas D. G., Cora S. A., 2001, *MNRAS*, 325, 34  
 Moustakas J., Kennicutt R. C., Tremonti C. A., Dale D. A., Smith J.-D. T., Calzetti D., 2010, *ApJS*, 190, 233  
 Nikolic B., Cullen H., Alexander P., 2004, *MNRAS*, 355, 874  
 Patton D. R., Ellison S. L., Simard L., McConnachie A. W., Mendel J. T., 2011, *MNRAS*, 412, 591  
 Peebles M. S., Pogge R. W., Stanek K. Z., 2009, *ApJ*, 695, 259  
 Perez M. J., Tissera P. B., Scannapieco C., Lambas D. G., de Rossi M. E., 2006, *A&A*, 459, 3  
 Rupke D. S. N., Veilleux S., Baker A. J., 2008, *ApJ*, 674, 172  
 Rupke D. S. N., Kewley L. J., Barnes J. E., 2010a, *ApJ*, 710, L156  
 Rupke D. S. N., Kewley L. J., Chien L.-H., 2010b, *ApJ*, 723, 1255  
 Sawala T., Guo Q., Scannapieco C., Jenkins A., White S. D. M., 2011, *MNRAS*, 413, 659  
 Scannapieco C., Tissera P. B., White S. D. M., Springel V., 2005, *MNRAS*, 364, 552  
 Scannapieco C., Tissera P. B., White S. D. M., Springel V., 2006, *MNRAS*, 371, 1125  
 Scannapieco C., Tissera P. B., White S. D. M., Springel V., 2008, *MNRAS*, 389, 1137  
 Scannapieco C., White S. D. M., Springel V., Tissera P. B., 2011, *MNRAS*, submitted (arXiv:1105.06805)  
 Sérsic J. L., Pastoriza M., 1967, *PASP*, 79, 152  
 Sol Alonso M., Michel-Dansac L., Lambas D. G., 2010, *A&A*, 514, A57  
 Springel V., 2005, *MNRAS*, 364, 1105  
 Teyssier R., Chapon D., Bournaud F., 2010, *ApJ*, 720, 149  
 Thielemann F.-K., Nomoto K., Hashimoto M., 1993, in Prantzos N., Vangioni-Flam E., Casse N., eds, *Origin and Evolution of the Elements*. Cambridge Univ. Press, Cambridge, p. 297  
 Tinsley B. M., Larson R. B., 1978, *ApJ*, 221, 554  
 Tissera P. B., 2000, *ApJ*, 534, 636  
 Toomre A., Toomre J., 1972, *ApJ*, 178, 623  
 Tremonti C. A. et al., 2004, *ApJ*, 613, 898  
 Woods D. F., Geller M. J., Barton E. J., 2006, *AJ*, 132, 197  
 Woosley S. E., Weaver T. A., 1995, *ApJS*, 101, 181  
 Zaritsky D., Kennicutt R. C., Jr, Huchra J. P., 1994, *ApJ*, 420, 87

This paper has been typeset from a  $\text{\TeX}/\text{\LaTeX}$  file prepared by the author.